

The influence of gas on the structure of merger remnants

Thorsten Naab^{1,2*}, Roland Jesseit¹ and Andreas Burkert¹

¹Universitäts Sternwarte München, Scheinerstr.1, D-81679 München, Germany

²Institute of Astronomy, Madingley Road, Cambridge, CB3 0HA, UK

Accepted ???. Received ??? in original form ???

ABSTRACT

We present a large set of merger simulations of early-type disc galaxies with mass ratios of 1:1 and 3:1 and 10% of the total disc mass in gas. The internal orbital structure and the kinematic and photometric properties of the remnants are analysed in detail and compared to pure stellar mergers. In contrast to the collisionless case equal-mass mergers with gas do not result in very boxy remnants which is caused by the suppression of box orbits and the change of the projected shape of minor-axis tube orbits in the more axisymmetric remnants. The isophotal shape of 3:1 remnants and the global kinematic properties of 1:1 and 3:1 remnants are only weakly affected by the presence of gas. 1:1 remnants are slowly rotating whereas 3:1 remnants are fast rotating and discy. The shape of the stellar LOSVD is strongly influenced by gas. Within the effective radius the LOSVDs of collisionless remnants have broad leading wings while their gaseous counterparts show steep leading wings, more consistent with observations of elliptical galaxies. We show that this change is also caused by the suppressed populating of box orbits and it is amplified by the formation of extended gas discs in the merger remnants which might eventually turn into stars. If elliptical galaxies have formed from mergers our results indicate that massive, slowly rotating boxy elliptical galaxies can not have formed from dissipative mergers of discs. Pure stellar (dry) mergers are the more likely candidates. On the other hand lower mass, fast rotating and discy ellipticals can have formed from dissipative (wet) mergers of early-type discs. So far, only unequal-mass disc mergers with gas can successfully explain their observed substructure. This is consistent with the revised morphological classification scheme of increasing importance of gas dissipation when moving from boxy ellipticals to discy ellipticals and then to spiral galaxies, proposed by Kormendy & Bender.

Key words: methods: analytical – methods: N-body simulations – galaxies: elliptical and lenticular, cD – galaxies: formation – galaxies: evolution – galaxies: fundamental parameters

1 INTRODUCTION

Inspired by the work of Toomre & Toomre (1972) a large number of simulations have been performed to investigate whether giant elliptical galaxies can be formed by binary mergers of disc galaxies. If this formation is correct the properties of the merger remnants would have to be in agreement with all observed properties of elliptical galaxies: their global kinematic and photometric properties as well as their fine-structure. Violent relaxation (Lynden-Bell 1967; Arad & Johansson 2005) of the stellar and dark matter components is the dominant dynamical process in the rapidly varying potential of an ongoing merger. However, it does not completely erase the information about the pro-

genitor galaxies. Therefore we should observe signposts of the formation process in the remnants, e.g. the morphology of the progenitor galaxies or the encounter geometry, both in the dynamics and the photometric properties. Elliptical galaxies, if they have formed this way, should show similar properties, providing information about the properties of their progenitors.

Collisionless simulations of equal mass mergers of disc galaxies have been studied in great detail by several authors (e.g. Gerhard 1981; Barnes 1992; Hernquist 1992; Naab & Burkert 2003, hereafter NB03, González-García & Balcells 2005, Jesseit et al. 2005 hereafter JNB05, Naab & Trujillo 2006, González-García & Balcells 2005). The global properties of the remnants are in agreement with observations of giant elliptical galaxies in the intermediate mass range,

* E-mail: naab@usm.lmu.de

e.g. equal mass remnants are slowly rotating, anisotropic, have boxy or discy isophotes. Unequal mass mergers are more isotropic and have discy isophotes (NB03). Merger remnants in general have phase space densities and surface density profiles that resemble observed ellipticals if bulges are added to the progenitor discs (Hernquist et al. 1993; Naab & Trujillo 2006).

As soon as the kinematics of simulated merger remnants was investigated in more detail, an interesting disagreement with observed elliptical galaxies was revealed. The line-of-sight velocity distributions (LOSVD) within the effective radius of merger remnants in general show small asymmetric deviations from Gaussian shape. They tend to have a steep trailing wing (Bendo & Barnes 2000; Naab & Burkert 2001b). In contrast, most observed rotating ellipticals clearly show a steep leading wing in their LOSVDs (Bender et al. 1994). Theoretically, axisymmetric, rotating one-component systems in fact show such a behaviour (Dehnen & Gerhard 1994). This would indicate that ellipticals are very simple one component systems that did not form by mergers, It is, however, unlikely that elliptical galaxies are such simple systems (see e.g. Emsellem et al. 2004). An alternative explanation, based on photometric and kinematical observations, is that rotating ellipticals contain embedded large scale stellar discs (e.g. Rix & White 1990; Scorza et al. 1998; Rix et al. 1999). A superposition of two distinct components, e.g. a hot spheroidal bulge and a rotationally supported cold disc, can also result in a steep leading wing of the LOSVD (Bender et al. 1994). Naab & Burkert (2001b) showed that embedding an exponential stellar disc artificially in collisionless merger remnants would change the asymmetries in the LOSVDs, leading to a good agreement with observations. Those discs need a scale length similar to the effective radius of the bulge and 10% -20% of its mass.

Such an extended disc naturally forms in merger remnants from high angular momentum gas located in the outer regions of the progenitors after it has been expelled along the tidal arms (Naab & Burkert 2001a; Barnes 2002; Springel & Hernquist 2005; Wetzstein et al. 2005). Gas initially located at smaller radii shocks and falls to the center of the remnant probably causing a starburst and/or feeding a super-massive black hole (Mihos & Hernquist 1996; Springel et al. 2005). This gas does not contribute to the extended disc. It has been shown by Bekki (1998) using simulations including gas and star formation that rotating lenticular galaxies with a disc like component can form from unequal-mass disc mergers. Furthermore, Springel & Hernquist (2005) has demonstrated with a simulation including star formation and feedback that a remnant with a dominant stellar discs can form self-consistently in an equal-mass merger of two gaseous discs. However, those initial conditions might be more typical for high redshift discs and for such an extreme case starformation can not be neglected.

In this paper we present simulations of disc galaxy mergers with small gas fractions of 10% which are more similar to low redshift discs. Our aim is to understand the influence of a small dissipative component (which will always exist, even if star formation is considered) on the global structure of mergers remnants. This will help to constrain the importance of additional physical processes like star formation, black-hole accretion and feedback (e.g. Cox et al.

2005; Springel & Hernquist 2005; Robertson et al. 2006). It has been shown by Barnes & Hernquist (1996) that the presence of gas influences the stellar component of the merging galaxies. Gas that accumulates at the center of merger remnants changes the central potential and can increase the velocity dispersion of the stars. Robertson et al. (2006) have demonstrated this effect in merger simulations including star formation. In addition, a steeper central potential well results in a more axisymmetric central shape of the remnants (Barnes 1998). At the same time the fraction of stars on box orbits is significantly reduced and tubes become the dominant orbit family (Barnes & Hernquist 1996). The most reasonable explanation for this behaviour is that systems with steep cusps in their potential can not sustain a large population of box orbits (Gerhard & Binney 1985; Schwarzschild 1993; Merritt & Fridman 1996; Valluri & Merritt 1998; Barnes 1998).

In this paper we present a new and more detailed analysis. With respect to resolution, statistical completeness and comparison to observations our study goes beyond previous investigations of similar simulations (e.g. Negroponete & White 1983; Barnes 1992; Barnes & Hernquist 1996; Bendo & Barnes 2000). We show quantitatively how a dissipative component changes the LOSVDs and the photometric properties of the merger remnants and explain in detail how these changes are connected to the changes of the orbital content of the remnants (see JNB05 for collisionless remnants). In particular, we demonstrate that a dissipative component can explain the origin of the observed asymmetries in the LOSVDs of elliptical galaxies. This paper is accompanied by a detailed two-dimensional kinematic analysis of the remnants presented here (Jesseit et al. 2006).

The paper is organised as follows. Section 2 presents the details of the simulations. A short overview of observable properties of ongoing mergers is given in Section 3. The intrinsic and projected shapes of the remnants and their orbital content are discussed in Section 4. In Section 5 we show the projected photometric and kinematic properties of the remnants followed by a detailed investigation of the LOSVDs in Section 6. A summary and conclusions follow in Section 7.

2 THE MERGER MODELS

Disc galaxies were constructed in dynamical equilibrium using the method described by Hernquist (1993). The system of units was: gravitational constant $G=1$, exponential scale length of the larger progenitor disc $h_d = 1$ (the scale height was $h_z = 0.2$) and mass of the larger disc $M_d = 1$. The discs were exponential with an additional spherical, non-rotating bulge with mass $M_b = 1/3$, a Hernquist density profile (Hernquist 1990) and a scale length $r_b = 0.2h_d$, and a pseudo-isothermal halo with a mass $M_d = 5.8$, cut-off radius $r_c = 10h_d$ and core radius $\gamma = 1h$. The parameters for the individual components were the same as for the collisionless mergers presented in NB03. Scaled to the Milky Way, one length unit is $3.5kpc$, one velocity unit is $262km/s$ and the mass unit is $5.6 \times 10^{10}M_\odot$. For this study we re-simulated the full set of 1:1 and 3:1 mergers with an addi-

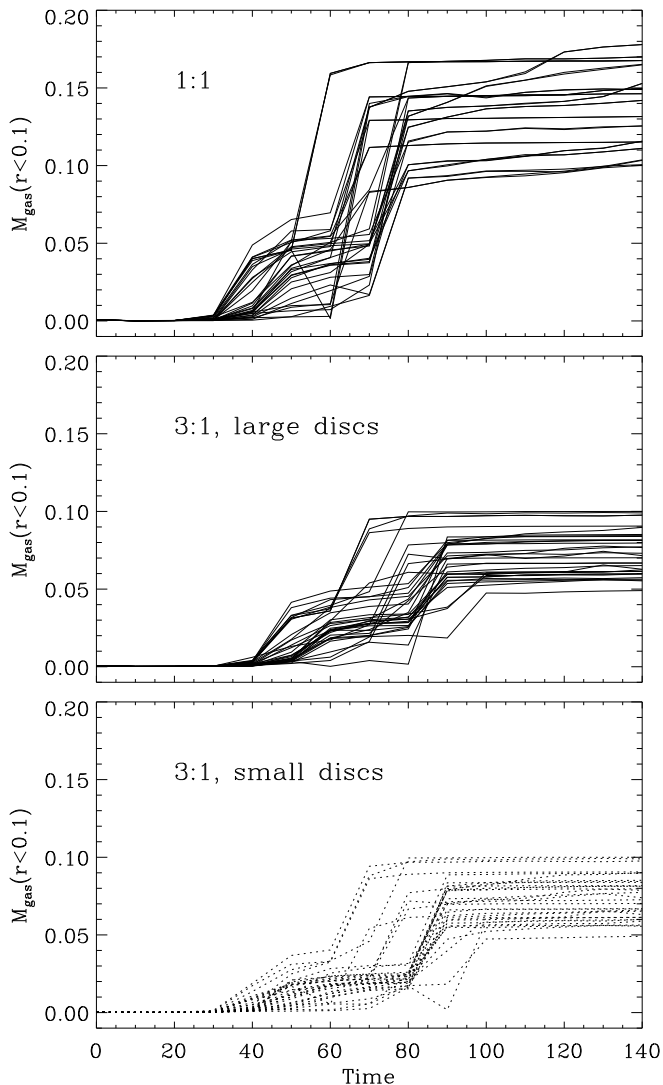


Figure 1. Time evolution of the gas mass inside a radius of $r = 0.1$ of the galaxies for 1:1 mergers (top panel) and the large (middle panel) and small (bottom panel) progenitor galaxies of 3:1 mergers. The central region of each galaxy has been followed separately. As the galaxies merge the enclosed masses become identical. The total initial gas mass of the more massive discs is $M_{\text{gas}} = 0.1$ and $M_{\text{gas}} = 0.0333$ for the less massive discs.

tional gas component in the disc. We replaced 10% of the stellar disc by gas with the same scale length and an initial scale height of $h_{z,\text{gas}} = 0.1h_z$. The gas was represented by SPH particles adopting an isothermal equation of state, $P = c_s^2 \rho$, with a fixed sound speed of $c_s = 0.039$ in velocity units, corresponding to $c_s \approx 10 \text{ km/s}$ if scaled to a Milky Way type galaxy. Assuming an isothermal equation of state implies that additional heat created in shocks, by adiabatic compression and feedback processes is radiated away immediately. It also implies that substantial heating processes prevent the gas from cooling below its effective temperature, e.g. sound speed. Recently, a number of simulations have shown that using an isothermal equation of state is a reasonably good approximation to the ISM in disc galaxies

(see e.g. Naab & Burkert 2001a; Barnes 2002; Li et al. 2005 and references therein).

We followed mergers of discs with mass ratios of $\eta = 1$ and $\eta = 3$ where η is the mass of the more massive galaxy divided by the mass of the merger partner. The equal-mass mergers were calculated adopting in total 440000 particles with each galaxy consisting of 20000 bulge particles, 60000 stellar disc particles, 20000 SPH particles representing the gas component in the disc, and 120000 halo particles. We decided to use twice as many halo particles than disc particles to reduce heating and instability effects in the disc components (Naab et al. 1999) by encounters between halo and disc particles. For the mergers with $\eta = 3$ the parameters of the more massive galaxy were as described above. The low-mass companion contained a fraction of $1/\eta$ the mass and the number of particles in each component, with a disc scale-length (stars and gas) of $h = \sqrt{1/\eta}$, as expected from the Tully-Fisher relation (Pierce & Tully 1992).

The N-body/SPH simulations were performed using the hybrid N-body/SPH treecode VINE (Wetzstein et al., in preparation) with individual timesteps. The gravitational forces were softened with a Spline kernel of $h_{\text{grav}} = 0.05$. The minimal size of the Spline kernel used for computing the SPH properties, h_{SPH} , was fixed to the same value. Implicitly, this procedure suppressed gas collapse on scales smaller than the softening scale and prevents numerical instabilities (Bate & Burkert 1997). All simulation have been run on a cluster of 64 1.5GHz Sun CPUs at the Institute of Astronomy in Cambridge.

The initial discs were run in isolation for two dynamical times to allow the systems to finally settle into an equilibrium state. In the merger the galaxies approached each other on nearly parabolic orbits with an initial separation of 30 length units and a pericenter distance of 2 length units. A study of orbits of merging dark matter halos in cosmological large scale simulations by Khochfar & Burkert (2006) has shown that a significant number of the merging halos are indeed on parabolic orbits with a broad distribution of pericenter distances. In this study we focus on the usually in simulations considered regime of small pericenter distances. In selecting unbiased initial parameters for the disc inclinations we followed the procedure described by Barnes (1998). The initial orientations for the discs were the same as in NB03, Table 1. The merger remnants were allowed to settle into dynamical equilibrium for approximately 30 dynamical time-scales after the merger was complete. Then their equilibrium state was analysed.

3 COMMENTS ON MERGER DYNAMICS AND GAS INFLOW

The properties of the initial disc galaxies change dramatically during the interaction. Tidal forces lead to the formation of tidal arms and trigger gas inflow to the center. The stellar systems are dynamically heated and finally merge into a new type of galaxy. Most investigations have focused on the properties of the final merger remnants. However, recent high resolution observations of nearby interacting galaxies have made it possible to compare ongoing mergers directly to different phases of simulated interactions (Dasyra et al. 2006).

It has not been investigated in detail during which phases of the mergers e.g. the central velocity dispersion or the effective radius adjusts to its final value. A detailed knowledge of how important observables evolve helps to constrain measurements of e.g. the mass-ratios of observed disc mergers (Dasyra et al. 2006), their gas accretion history, or their starformation rates.

We measured the observables, in particular the effective velocity dispersion of the progenitor discs, during the interaction by following every individual galaxy analysing snapshots of the merger in the orbital plane every 10 unit times (approximately every 10 half-mass rotation periods of the more massive disc). To perform the analysis as consistent as possible with observations (see Dasyra et al. 2006) we computed the effective radius r_{eff} of every galaxy as the projected spherical half-mass radius of the stellar particles within 5 length scales only taking particles of the galaxy itself into account. Thereby we avoided unrealistically large values for r_{eff} when the galaxies overlap. The effective central stellar velocity dispersion σ_{eff} for each galaxy was then computed within $0.5r_{\text{eff}}$ taking all stellar particles into account. To follow the gas accretion onto the center we computed the total gas mass within a radius of $r = 0.1$, $M_{\text{gas}}(r < 0.1)$, which is two times the gravitational Spline softening length of the simulations, $h_{\epsilon} = 0.05$.

In Fig. 1 we show the amount of gas accreted onto the center of each galaxy. Every line corresponds to one disc galaxy. As soon as the galaxies merge (at $t \approx 70$) the two lines of the progenitor galaxies join. In general equal mass galaxies merge faster than unequal mass galaxies. For 1:1 mergers every galaxy contains $M_{\text{gas}} = 0.1$. After the first encounter between 10% and 60% of the available gas in the progenitor discs is funneled to the center. In some cases additional gas, expelled from the partner galaxy, is captured already at early phases of the merger. The exact numbers vary with the encounter geometry. In general, gas transport is more effective if the spin and the orbital angular momentum of the disc is aligned (Barnes 2002). After the galaxies have merged between 50% and 85% for 1:1 mergers (between 40% and 75% for 3:1 mergers) of the gas has accumulated at the center.

To test the effect of halo resolution on the gas inflow we have re-run two 1:1 and 3:1 mergers with very different geometries, respectively, changing the halo properties in two ways: First we have changed the softening of the halo to $\epsilon_{\text{halo}} = 0.09$ and the gas softening to $\epsilon_{\text{gas}} = 0.03$ to scale as the square root of the particle mass. This guarantees that the maximum gravitational force exerted from a particle is independent of its mass (Dehnen 2001). The effect of this change on the gas properties was very small and we could not find a general trend.

Secondly we used the original halo softening ($\epsilon_{\text{halo}} = \epsilon = 0.05$) and increased the mass resolution of the more massive halo to 348000 particles to get the same individual particle masses in all collisionless components. For this set of simulations we found that dissipational effects are slightly enhanced. The amount of gas driven to the center is increased by 5% to 15%. In Fig. 5 we show the cumulative gas mass distribution of one 1:1 and on 3:1 merger in comparison to the original simulation. Most likely the higher halo resolution reduces the effect of artificial two-body heating by encounters of halo and gas particles. The global effect

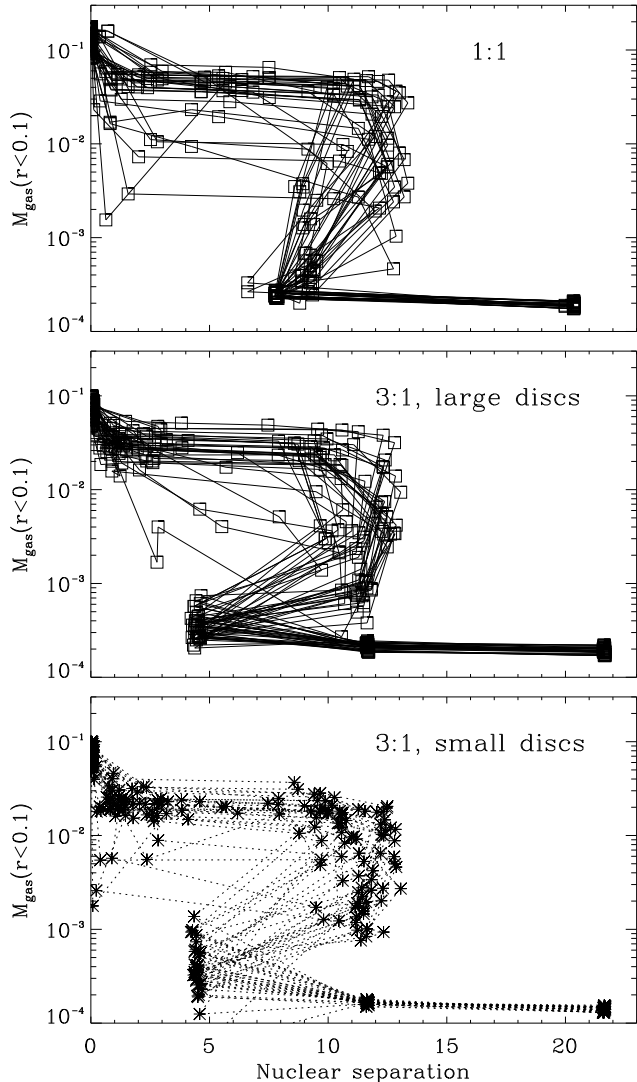


Figure 3. Gas mass inside a radius of $r = 0.1$ of the galaxies for 1:1 mergers (top panel) and the large (middle panel) and small (bottom panel) progenitor galaxies of 3:1 mergers as a function of nuclear separation.

on the gas distribution is, however, small and the stellar remnants are only weakly affected (see Section 4). Based on these results and to be fully consistent with the already performed collisionless simulations we have used a gravitational softening of $\epsilon = 0.05$ for all components.

In Fig. 2 we show the final gas distribution for 1:1 and 3:1 mergers with three different encounter geometries. For 1:1 remnants the gas can be distributed in warped discs or more irregular structures like polar rings. 3:1 remnants show a more regular disc structure. The formation of extended gas discs in 3:1 merger remnants has been predicted by Naab & Burkert (2001a) and we refer to Barnes (2002) who has studied the dynamics of disc formation extensively. In Fig. 3 we show the central gas content as a function of nuclear separation of the merging galaxies. The main accretion phases are after the first encounter and at the final merger of the galaxies (see e.g. Mihos & Hernquist 1996).

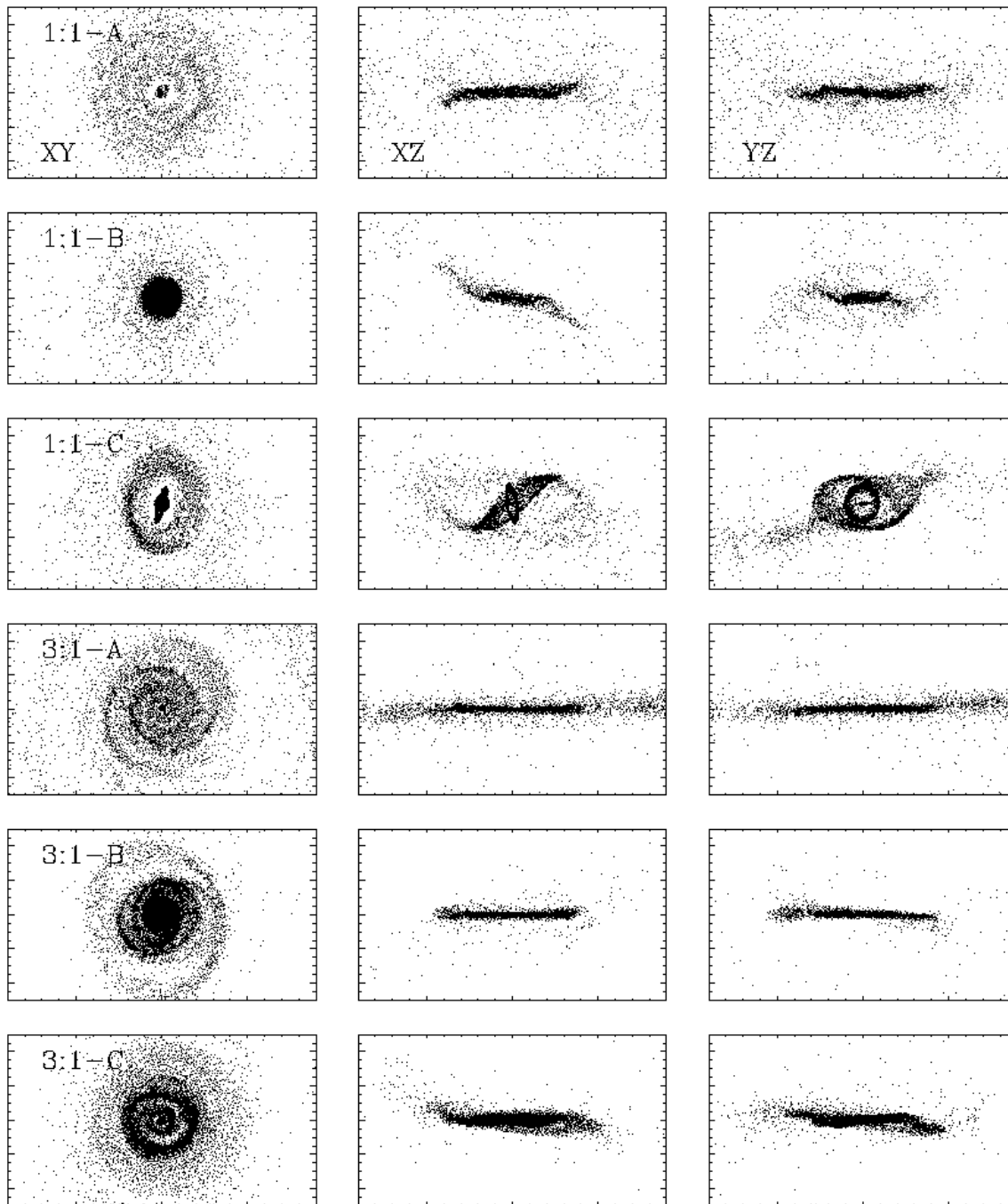


Figure 2. Final gas distribution for 1:1 and 3:1 remnants with three different geometries A, B, and C seen along the principal axes of the main stellar bodies. The box length is 8 unit lengths in vertical direction and 18 unit lengths in horizontal direction. Most remnants have embedded gas discs with a more regular disc structure for 3:1 remnants.

It is important to note for comparisons with observations that the central gas content differs significantly before and after the first encounter although the galaxies can have the same nuclear separation. This fact could be used as additional diagnostics to predict in which state of the merger observed galaxies are. The effective velocity dispersion versus nuclear separation is plotted in Fig. 4. Similar to the gas content the dispersion rises in two phases: after the first en-

counter and, to its new equilibrium value, in the final merger phase. In combination with the evolution of the effective radii these results have been used to test dynamical mass estimates of observed nearby ULIRGs in interacting pairs (Dasyra et al. 2006) which all appear to have mass ratios between 1:1 and 3:1. Our results also indicate that merging disc galaxies might already fall on the observed black-hole

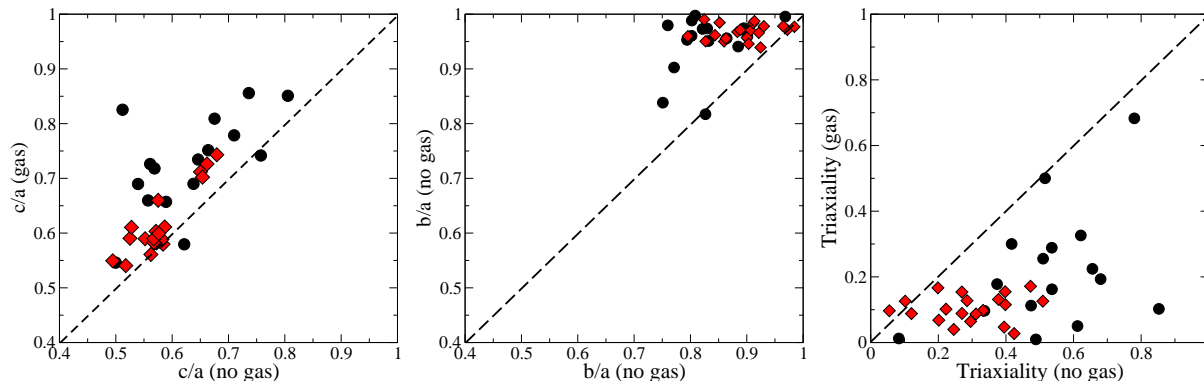


Figure 6. Axis ratios of the stellar remnants for the simulations with and without gas for mass ratios 1:1 (black dots) and 3:1 (red diamonds) *Left panel:* ratio between the short and the long axis (c/a). *Middle panel:* ratio between the intermediate and the long axis (b/a). *Right panel:* triaxiality of the stellar remnants. Stellar remnants with a gas component are less triaxial with a similar maximum flattening (c/a).

mass - sigma relation (Tremaine et al. 2002) soon after their first encounter (Dasryra et al., submitted).

4 INTRINSIC SHAPES AND STELLAR ORBITS OF THE MERGER REMNANTS

The intrinsic shape of a mass distribution is defined by the ratio of its three principal axes. They were determined by diagonalising the moment of inertia tensor of each merger remnant. The particles were binned according to their binding energy. That ensures that the subsets of particles follow the structure of the remnant naturally (Weil & Hernquist 1996). The triaxiality parameter T is defined as

$$T = \frac{1 - (b/a)^2}{1 - (c/a)^2}, \quad (1)$$

where a , b , and c are the long, intermediate and minor-axis, respectively. The shape of merger remnants is closely related to their intrinsic orbital structure as shown by JNB05. In general minor-axis tubes are more heavily populated in oblate remnants and box orbits are most abundant in remnants triaxial remnants with $T = 0.5$ (see Fig. 5 and Fig. 6 of JNB05). In Fig.6 we show how the presence of gas influences the intrinsic shapes of the stellar components of the merger remnants. The triaxiality is lowered for almost every remnant due to the influence of gas. 3:1 remnants with gas only reach a maximum triaxiality of $T = 0.2$, while in the collisionless case they can have triaxialities as large as $T = 0.5$. Although the triaxiality of the 1:1 remnants is also lowered substantially the effect is smaller than for 3:1 remnants. The more violent merging process can to some extent counter the dissipational influence of the gas. Gas rather makes the remnant more axisymmetric than more flattened (Fig.6). The ratio between the short and the long axis of the triaxial body (c/a) is only increased by $\sim 10\%$, making the remnant slightly more spherical. In contrast, for almost all remnants b/a is now close to unity, i.e. the systems are axisymmetric.

The classification of orbits follows the procedure presented in JNB05 (and references therein) and is based on the method developed by Carpintero & Aguilar (1998). We will repeat only the most important steps. After the merger

remnant had settled into equilibrium we froze the particle distribution and computed the potential using the Self Consistent Field (SCF) method (Hernquist & Ostriker 1992). As initial condition for the integration of the orbits we took the positions and velocities of the particles at the final snapshot of the simulation. With this method all orbit classes which exist in general triaxial potentials can be identified. The orbits were classified as minor-axis tubes, outer major-axis tubes, inner major-axis tubes, boxes and boxlets. About 5% -10% of all orbits in every remnant could not be classified with this procedure.

Every orbit class has distinct kinematical properties and shapes. Minor-axis tubes are the backbone of oblate and disc-like systems and have a non-vanishing angular momentum around the short axis of the potential. Major-axis tubes are found in prolate or nearly spherical systems with a non-vanishing angular momentum around the long axis. Boxes and boxlets have no mean angular momentum and can be found close to the center of the potential.

We compared the population of each orbit class averaged over all 1:1 and 3:1 mergers, respectively, for all merger remnants with and without gas. The result is shown in Fig. 7. In both, 1:1 and 3:1 mergers, gas drastically reduces the fraction of box orbits while the fraction of minor-axis tubes increases by a factor of 2-3 (the slightly larger central gas fractions of the simulations with higher halo resolution discussed in the previous section results in an increase of the tube orbit fraction of 3-5%). This confirms the observed trends towards an axisymmetric shape. Major-axis tubes are also de-populated which is consistent with the reduction of the prolateness. Box orbits are still found at the smallest radii, but minor-axis tubes in general start to be the dominant orbit class at smaller radii than in the dissipationless mergers (Fig.8). This finding is in agreement with Barnes & Hernquist (1996) and Barnes (1998).

The superposition of all stars, which are on different orbits, determine the projected photometric and kinematic properties of the remnants which are investigated in the following sections.

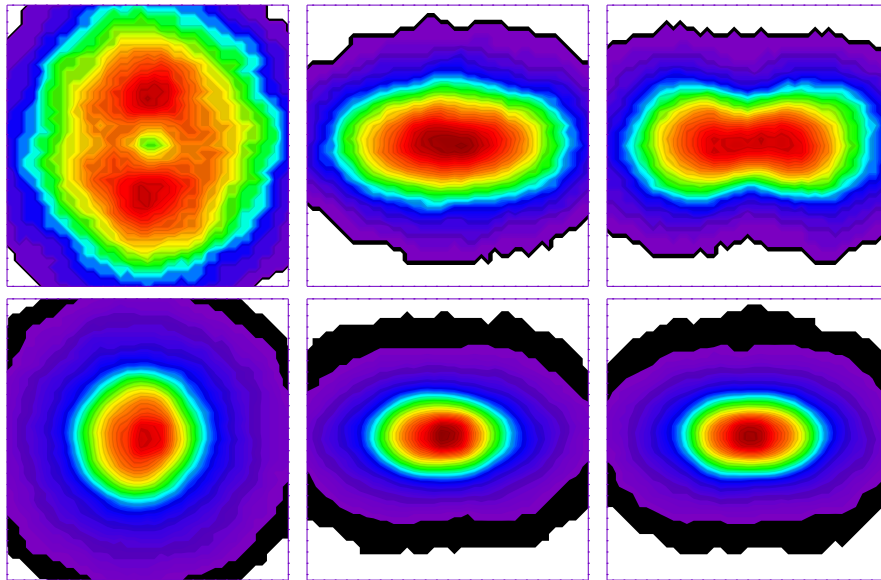


Figure 9. Typical projected surface density of stellar particles on minor-axis tube orbits for a triaxial collisionless 1:1 remnant (upper row) and its more oblate counterpart with gas (bottom row). From left to right we show projections along the short, intermediate, and long axis. The box length is $\approx 2r_{\text{eff}}$. Tube orbits, which dominate around the effective radius, support a boxy/peanut isophotal shape in the triaxial potential of the collisionless remnant. In the more axisymmetric potential of the remnant with gas the shape is less boxy or even discy.

5 GLOBAL PHOTOMETRIC AND KINEMATIC PROPERTIES

We have performed the isophotal and kinematic analysis of 500 random projections of every remnant following the procedure presented in NB03. An artificial image of each projected remnant was created by binning the stars within the central 10 length units into 128×128 pixels, smoothed with a Gaussian filter of standard deviation 1.5 pixels. The isophotes and their deviations from perfect ellipses were then determined using a data reduction package kindly provided by Ralf Bender. In this section the analysis was only performed for the stellar particles. In the following we refer to the stellar particle distribution as collisionless/without gas or dissipative/with gas depending on whether gas was present or not.

The characteristic ellipticity ϵ_{eff} for each projection is defined as the isophotal ellipticity at $1.5r_e$. In Fig. 10 we show the normalized histograms of the ellipticity distribution for the stellar 1:1 and 3:1 remnants with and without gas. The distributions look similar for 3:1 remnants, whereas 1:1 remnants with gas have more projections with small ellipticities as expected if the main stellar body is more axisymmetric. Still, the distributions peak at similar ellipticities as mainly the ratio of the intermediate to the long axis, b/a , is affected by the presence of gas (see Section 4).

The effective a_4 -coefficient, $a_{4\text{eff}}$, was computed as the mean value of a_4 between $0.25r_e$ and $1.0r_e$, with r_e being the projected spherical half-mass radius. In contrast to NB03 we do not use the maximum value of a_4 in case of a peaked distribution which did, however, not change the results. The normalized histograms of the $a_{4\text{eff}}$ distribution for all 1:1 and 3:1 remnants with and without gas is shown in Fig. 11. In contrast to the collisionless case the 1:1 remnants

with gas do not show a significant number of boxy projections any more. Their deviations from perfect ellipses has decreased. For 3:1 remnants the effect of the gas is weaker. There are now more projections which are significantly discy, with $a_{4\text{eff}} > 2$.

The most important physical reason for the lack of boxy projections for mergers with gas is the different behaviour of minor-axis tube orbits in axisymmetric and triaxial potentials. As we have shown in Section 4, collisionless 1:1 remnants are more triaxial whereas stellar 1:1 remnants with gas are more axisymmetric. Minor-axis tube orbits in triaxial potentials can support a boxy/peanut isophotal shape in the projection along the minor axis and, more importantly, along the long axis (see Fig. 11 in JNB05). Minor-axis tubes are the dominant orbit family around the effective radius of the collisionless remnants (see Fig. 8) and therefore are largely responsible for the overall isophotal shape (see NB03 and JNB05). In the more axisymmetric potentials of the remnants with gas the minor-axis tubes look more elliptical/less boxy or even discy in all projections. This behaviour is qualitatively demonstrated in Fig. 9 for a typical 1:1 remnant. In addition, the fraction of box orbits and boxlets, which can support a boxy shape at the center of collisionless remnants (see Fig. 11 in JNB05) is significantly reduced (Fig. 8).

The central velocity dispersion σ_0 of every remnant was determined as the average projected velocity dispersion of the luminous particles inside a projected galactocentric distance of $0.2r_e$ and we defined the characteristic rotational velocity along the major axis, v_{maj} , and the minor-axis, v_{min} , as the rotational velocity at $1.5r_e$ and $0.5r_e$, respectively. The amount of minor-axis rotation was parameterized as $v_{\text{min}}/\sqrt{v_{\text{maj}}^2 + v_{\text{min}}^2}$ (Binney 1985). Minor-axis rotation in

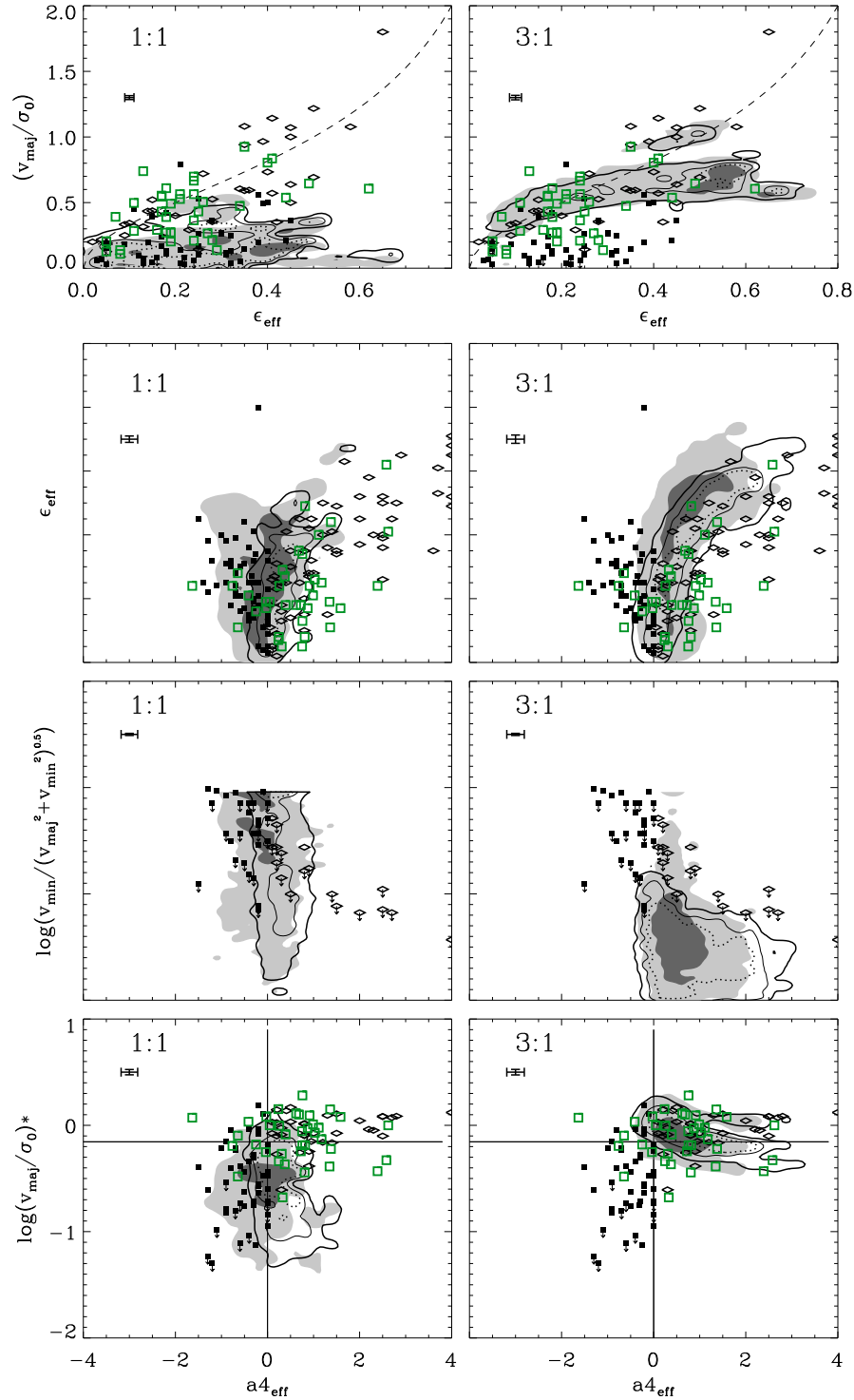


Figure 12. Global photometric and kinematic properties of the stellar components of 1:1 and 3:1 merger remnants with and without gas. The contours indicate areas of 50% (dotted line), 70% (thin line) and 90% (thick line) probability to detect a merger remnant with gas with the given properties. For comparison, the shaded areas indicate the 50% (dark grey) and 90% (bright grey) probabilities for collisionless remnants. Data for observed boxy (filled squares) and discy (open diamonds) ellipticals have been kindly provided by Ralf Bender. Data for local merger remnants (open green squares) are taken from Rothberg & Joseph (2006). From top to bottom we show: ellipticity, ϵ_{eff} , versus v_{maj}/σ_0 (the theoretical value for a spheroid flattened by rotation is shown by the dashed line); effective isophotal shape, $a4_{\text{eff}}$, versus ϵ_{eff} , versus the amount of minor-axis rotation, $v_{\text{min}}/\sqrt{v_{\text{maj}}^2 + v_{\text{min}}^2}$, and versus the anisotropy parameter, $(v_{\text{maj}}/\sigma_0)^*$. The stellar components of remnants with gas (in particular 1:1) do not show boxy isophotes any more and the 3:1 remnants with gas are more discy and show less minor-axis rotation.

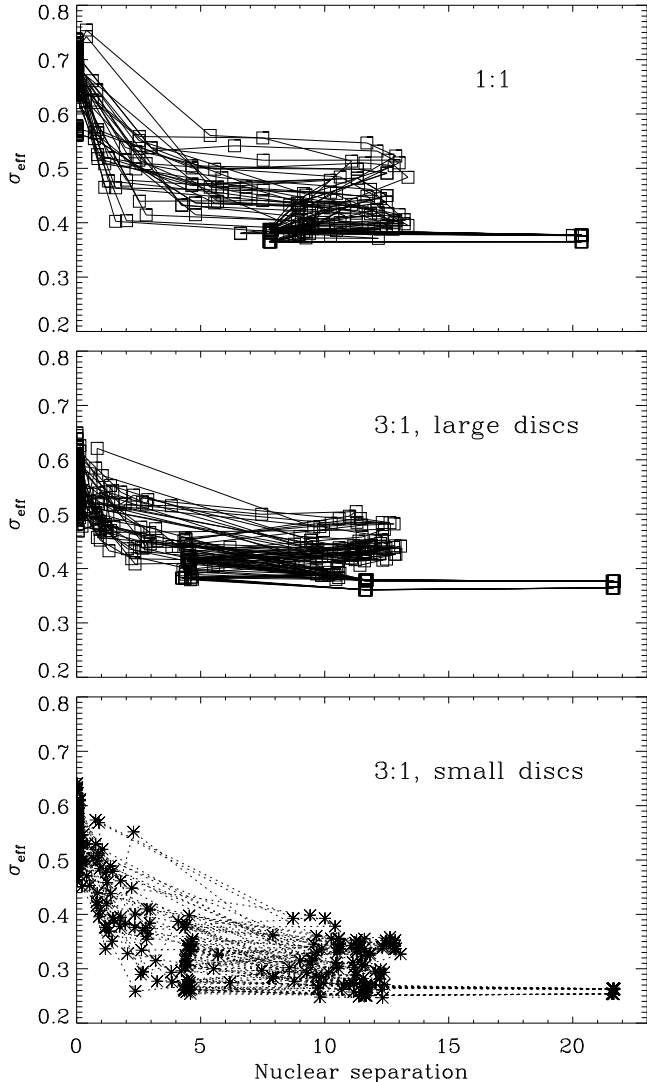


Figure 4. Effective stellar velocity dispersion, σ_{eff} , of the galaxies for 1:1 mergers (top panel) and the large (middle panel) and small (bottom panel) progenitor galaxies of 3:1 mergers as a function of nuclear separation.

elliptical galaxies, in addition to isophotal twist, has been suggested as a sign for a triaxial shape of the main body of elliptical galaxies (Wagner et al. 1988; Franx et al. 1991).

In Fig. 12 we summarize the properties of the stellar components of the 1:1 and 3:1 merger remnants with gas in comparison to the remnants without gas. The remaining gas is not included in this analysis. In the upper row we show the location of the remnants in the $v_{\text{maj}}/\sigma_0 - \epsilon_{\text{eff}}$ plane. There are no fundamental differences between remnants with and without gas. The dichotomy found by Barnes (1998), Naab et al. (1999) and NB03 that 1:1 mergers produce slowly rotating remnants and 3:1 remnants produce fast rotating remnants is not changed by the presence of gas. In general the properties of 1:1 and 3:1 remnants are in very good agreement with recent observations of (predominantly discy) nearby merger remnants

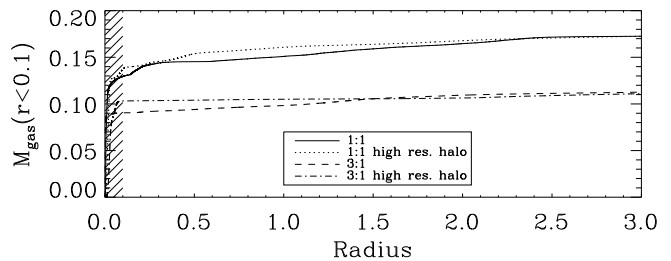


Figure 5. Comparison of the cumulative gas mass versus radius for a 1:1 (solid line) and a 3:1 merger (dashed line) and their counterparts with higher resolution in the halo component (dotted and dash-dotted line). The shaded area indicates the central part of the remnants. A better resolved halo results in a more concentrated gas distribution. The central gas content can increase by 15%.

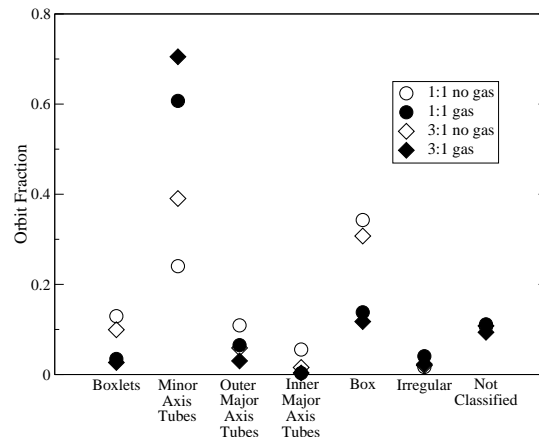


Figure 7. Mean orbit fractions for the 40% most tightly bound particles for all 1:1 (circles) and 3:1 (diamonds) remnants without (open symbols) and with gas (filled symbols).

by Rothberg & Joseph (2006) and discy and boxy elliptical galaxies.

The distribution of the remnants in the $\epsilon_{\text{eff}} - a_4$ plane is shown in the second row. As shown above the stellar components of 1:1 remnants with gas do not appear boxy any more and can not explain the formation of boxy ellipticals. For individual simulated mergers this trend was already found by Bekki & Shioya (1997) and thereafter rediscovered by Springel (2000). Without assuming additional physics for star formation all formerly boxy remnants are now close to elliptical (see Fig. 11). The agreement of 3:1 remnants with nearby merger remnants and discy elliptical galaxies is significantly better.

In the third row of Fig. 12 we compare the amount of minor-axis rotation as a function of the isophotal shape of the collisionless remnants and the remnants with gas. There is a weak trend for remnants with gas to show less minor-axis rotation than the collisionless counterparts. This finding can be understood as the fraction of major-axis tubes, which are mainly responsible for minor-axis rotation, is on average reduced due to the influence of gas (see Fig. 7).

The last row of Fig. 12 shows the location of the rem-

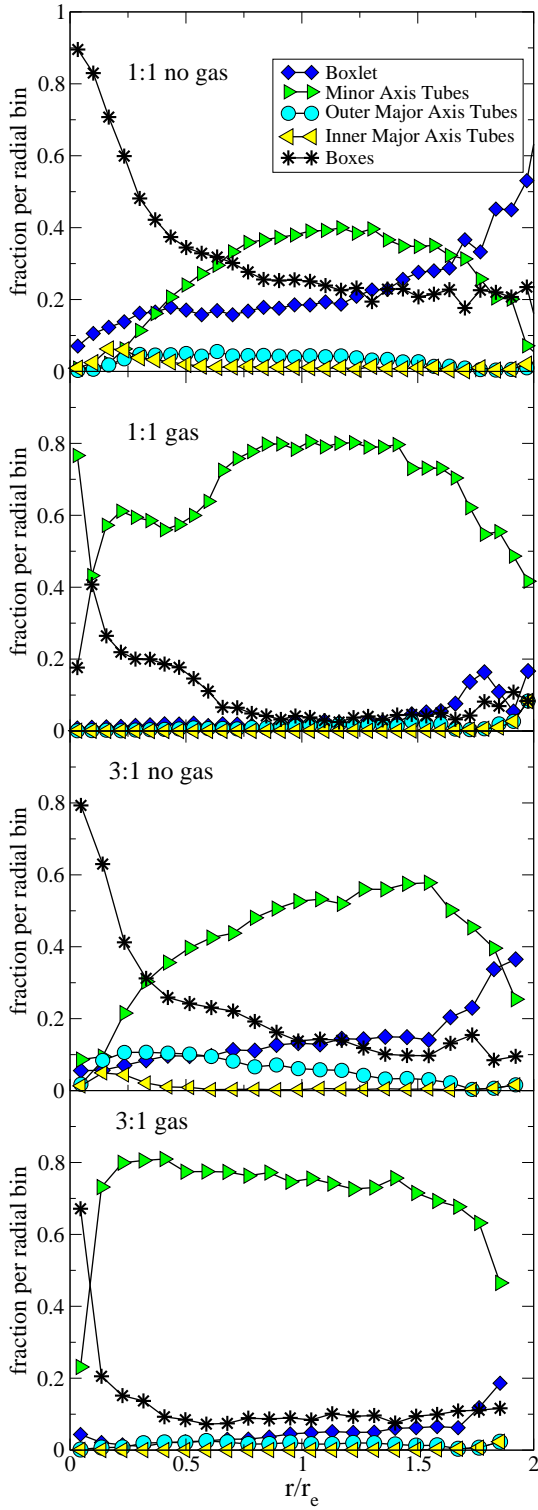


Figure 8. Fraction of particles on different orbits in radial bins in units of r_e for a typical 1:1 remnant without and with gas (two upper panels) and a typical 3:1 remnant with and without gas (two lower panels). Remnants with gas are more dominated by tube orbits.

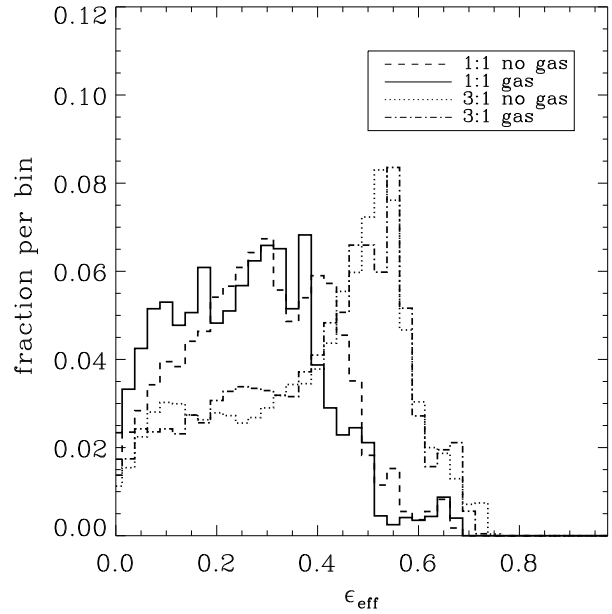


Figure 10. Distribution of the projected effective ellipticities, ϵ_{eff} for the stellar body of 1:1 remnants with (solid) and without (dashed) gas and for 3:1 remnants with (dashed-dotted) and without (dotted) gas.

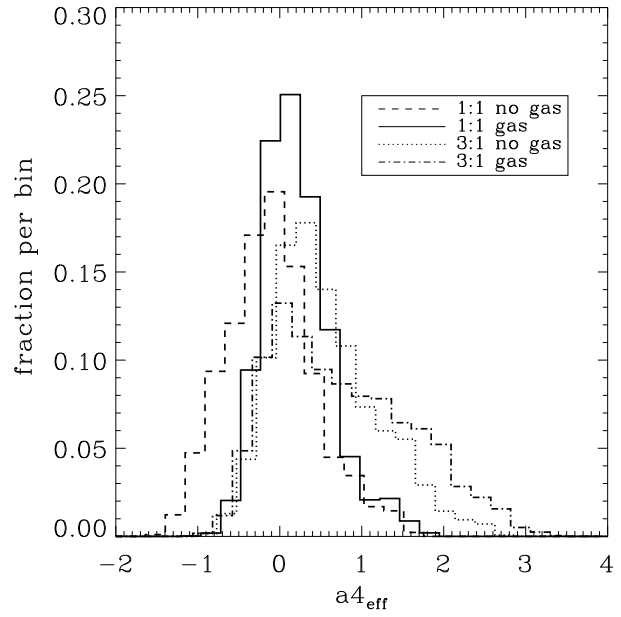


Figure 11. Distribution of the projected effective isophotal shape, $a_{4\text{eff}}$, of the stellar body for 1:1 remnants with (solid) and without (dashed) gas and for 3:1 remnants with (dashed-dotted) and without (dotted) gas.

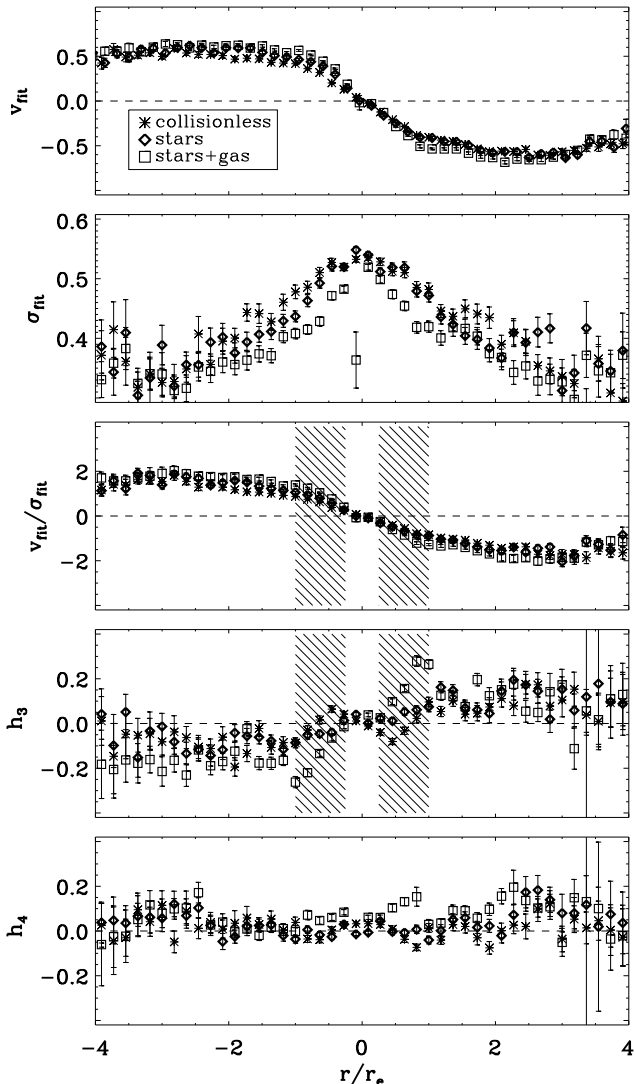


Figure 13. Kinematical properties of a typical 3:1 merger remnant (collisionless, stars, stars+gas). The shaded area indicates the radial range where the local correlations between h_3 and $v_{\text{fit}}/\sigma_{\text{fit}}$ have been measured (see Fig. 14). If gas is present during the merger, h_3 changes sign.

nants in the $(v_{\text{maj}}/\sigma_0)^* - a_4$ plane. Here $(v_{\text{maj}}/\sigma_0)^*$ is the traditional anisotropy parameter (Binney 1978, see Binney (2005); Burkert & Naab (2005) for a revised version of the anisotropy parameter and its application to N-body simulations). On average the 1:1 remnants with gas have slightly larger values of $(v_{\text{maj}}/\sigma_0)^*$. Boxy and anisotropic remnants which we found for collisionless remnants did not form. In addition, we find more projected gas-remnants with small $(v_{\text{maj}}/\sigma_0)^*$ but discy isophotes than for the pure collisionless remnants. In this regime no observed elliptical galaxies (Rothberg & Joseph 2006) can be found. However, there are some S0 galaxies with similar properties (Rix et al. 1992). A possible connection will be investigated in a subsequent paper. 3:1 remnants with gas have similar properties to their collisionless counterparts. Remnants of mergers with gas on average appear more discy and are in better agreement with observed discy ellipticals and nearby merger remnants.

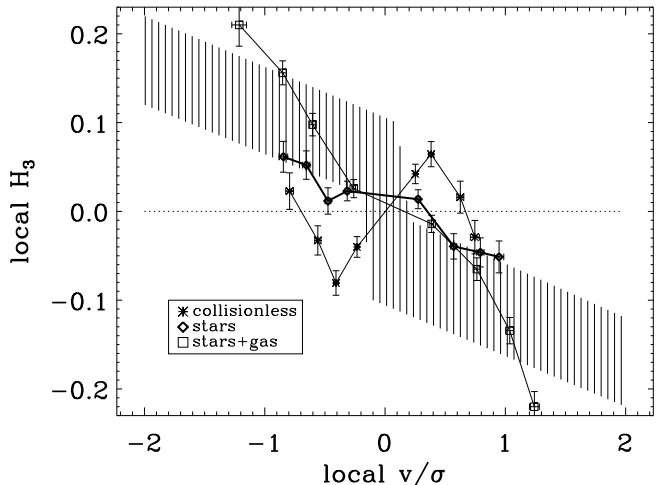


Figure 14. Local correlation between h_3 and v/σ for the same 3:1 remnants as in Fig. 13. The collisionless remnant shows an anti-correlation between for low v/σ and a correlation for the largest values. For the stellar remnant of the merger with gas h_3 and v/σ is anti-correlated. Including the gas in the analysis leads to a stronger anti-correlation in good agreement with observations. The range of the observational data is indicated by the shaded area.

6 LOSVD ANALYSIS OF THE MERGER REMNANTS

To measure the LOSVDs of a merger remnant we shifted the densest region of every two-dimensional projection to the origin and placed a slit with a width of 0.4 unit lengths along the apparent long axis of each projected remnant. The slit was then subdivided into grid cells of 0.15 unit lengths. Thereafter we binned all particles falling within each cell in velocity along the line-of-sight. The width of the velocity bins was set to a value of 0.2 for line-of-sight velocities v_{los} in the range $-4 \leq v_{\text{los}} \leq 4$. This resulted in 40 velocity bins over the whole velocity interval. Using the binned velocity data we constructed line-of-sight velocity profiles for each bin along the slit. Subsequently we parameterized deviations from the Gaussian shape using Gauss-Hermite basis functions (Gerhard 1993; van der Marel & Franx 1993). The kinematic parameters of each profile (σ_{fit} , v_{fit} , h_3 , h_4) were then determined by least squares fitting (see Cretton et al. 2001). The large number of simulated stellar particles (> 100000) guaranteed that at least 1000 particles fall within each bin inside the effective radius. We have analysed three sets of particle distributions: all star particles of the collisionless simulation, the star particles of the simulation with gas and, assuming that all gas particles have transformed into stars, stars and gas particles of the simulation with gas. In the following we refer to these sets of particles as: collisionless, stars, and stars+gas.

As a prototypical example Fig. 13 shows the observables v_{fit} , σ_{fit} , $v_{\text{fit}}/\sigma_{\text{fit}}$, h_3 , and h_4 together with the bootstrapping errors as a function of radius for a 3:1 merger remnant. We compare the kinematics of the collisionless remnant with the stars and stars+gas of the simulated remnant with gas. The line-of-sight velocity is only weakly affected by the presence of gas. There is a slightly steeper gradient at the cen-

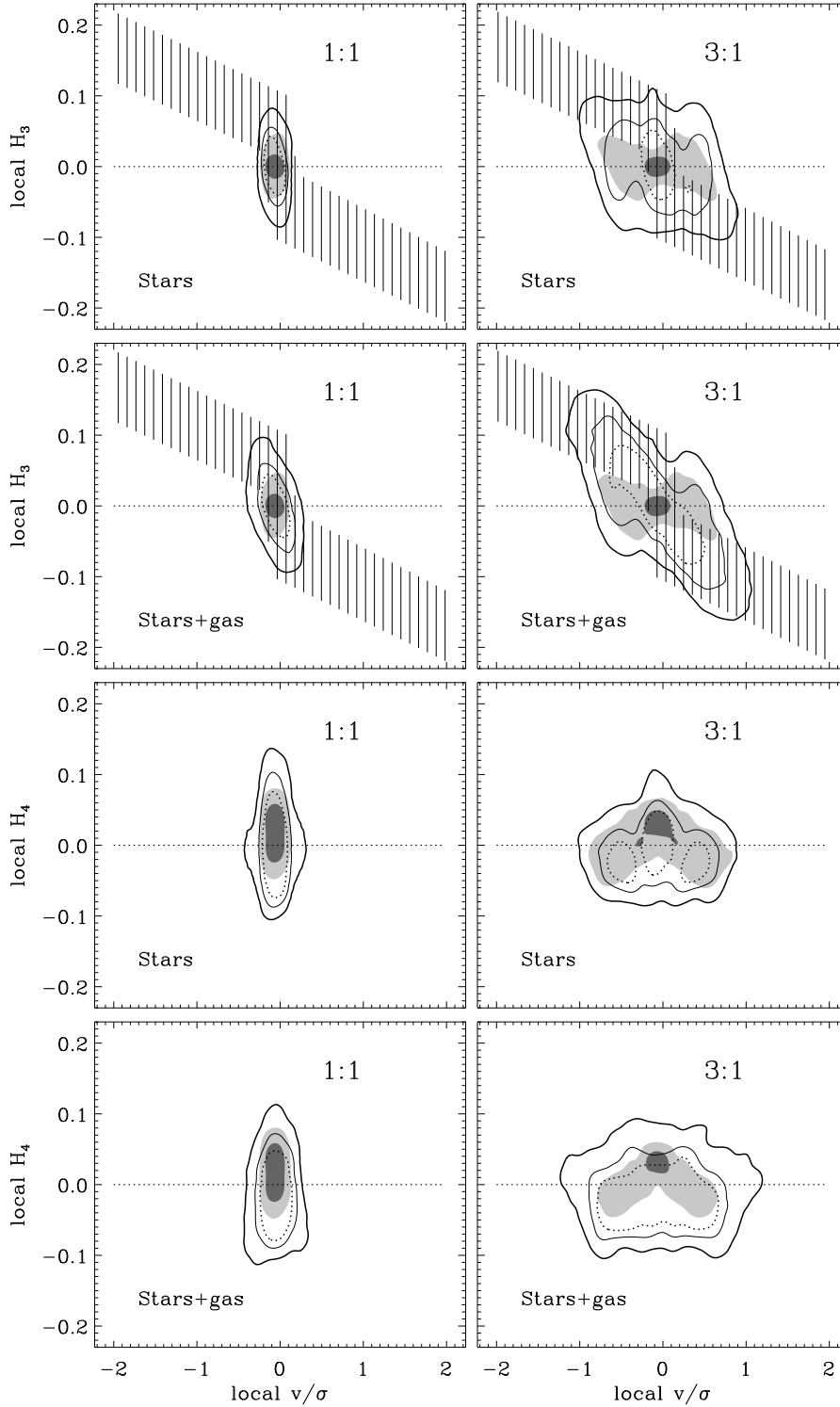


Figure 16. *Upper row:* Local correlation between h_3 and v/σ between 0.25 and $1r_e$ along the major axis for 1:1 and 3:1 merger remnants with and without gas. The contours are as in Fig. 12. The vertical lines indicate the location of observational data by Bender et al. (1994). The collisionless 1:1 remnants (left panel) rotate very slowly. The asymmetry of the LOSVD of the stars (h_3) increases if gas is added to the simulations. Collisionless 3:1 remnants do not show the observed anti-correlation (right panel, shaded area). The corresponding stellar components of the mergers with gas (contours) have larger maximum values of v/σ and show stronger asymmetries with a clear indication for a change in the tilt. *Second row:* Including the gas (assuming it has transformed into stars after the merger was complete) the distribution for equal mass remnants becomes weakly tilted (left panel) whereas the distribution for 3:1 remnants (right panel) shows a clear tilt and extends to a local $v/\sigma \approx 1$ in good agreement with observations. *Third row:* Same as above but for h_4 . Most collisionless remnants (shaded areas) have a positive local values of h_4 whereas the remnants with gas show equal amount of positive and negative values (contours). For 3:1 remnants there is a trend for regions with higher v/σ to have negative h_4 . *Bottom panel:* Adding gas to the analysis results in an over-all shift to more negative values of h_4 .

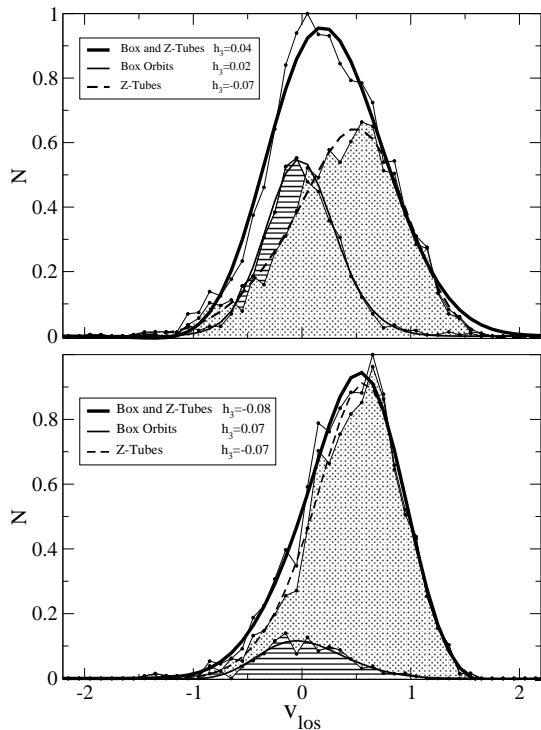


Figure 15. Typical normalised velocity profiles at $\approx 0.75r_{\text{eff}}$ of the dominant population of Z-tubes and box orbits for a collisionless 3:1 remnant (upper panel) and the stellar component of its counterpart with gas (lower panel). Z-tubes have a negative h_3 . In combination with the large fraction of box orbits of the collisionless remnant the overall LOSVD shows a broad leading wing. The remnant with gas is dominated by Z-tubes and has a steep leading wing, in agreement with observations of rotating elliptical galaxies.

ter for the merger with gas. The velocity dispersion profile (stars+gas) shows a clear signature of the extended gas disc: it decreases faster with increasing radius. At the center where the gas has formed a cold dense blob the differences in the dispersion are most significant.

The most interesting feature can be seen for h_3 which characterises the asymmetry of the LOSVD. In the collisionless case h_3 and v_{fit} have the same sign - and nearly the same slope - inside half an effective radius. Towards one effective radius the slope for h_3 changes and at larger radii v_{fit} and h_3 are anti-correlated (Fig. 13). This behaviour is typical for all 3:1 remnants (Naab & Burkert 2001b; Bendo & Barnes 2000) and it is in contradiction to observed elliptical galaxies (Bender et al. 1994) where h_3 and $v_{\text{fit}}/\sigma_{\text{fit}}$ are anti-correlated inside the effective radius (indicated by the shaded area in Fig. 14). The slope of the correlation between h_3 and $v_{\text{fit}}/\sigma_{\text{fit}}$ changes if gas is present during the merger. In the region of interest h_3 and $v_{\text{fit}}/\sigma_{\text{fit}}$ are now weakly anti-correlated for the stars and strongly anti-correlated for stars+gas (see Fig. 14). In Fig. 15 we show the velocity distribution and the Gauss-Hermite fits for box orbits and Z-tubes, which dominate the remnants. The collisionless 3:1 remnant is compared to its counterpart with gas (same initial orientation). For both remnants the Z-tubes have a negative h_3 which corresponds to a steep leading wing. In combination with the large fraction of box

orbits the resulting LOSVD of the collisionless remnant has a broad leading wing. Bendo & Barnes (2000) have shown a very similar distribution for their remnants. The stellar component of the remnant with gas has a much lower fraction of box orbits and the resulting LOSVD is dominated by the steep leading wing of the minor-axis tubes.

The fourth order coefficient, h_4 , characterizes a LOSVD that is more peaked than a Gaussian if positive and less peaked if negative (Fig. 13). For the 3:1 remnant chosen here h_4 appears to be positive at the center and negative around the effective radius, a feature that is less prominent for simulations with gas. In this paper we show the results for h_4 for completeness, however we will not discuss it in greater detail.

In Fig. 16 we have summarised the local correlations between h_3 and v/σ in the range of 0.25 to 1 r_e along the projected major axis for 500 random projections for all 1:1 and 3:1 merger remnants with and without gas. The collisionless 1:1 remnants (left panel) rotate very slowly and are consistent with observations. The asymmetry of the LOSVD of the stars (h_3) increases if gas is added to the simulations. Rotating collisionless 3:1 remnants do not show the observed anti-correlation (right panel, shaded area). The corresponding stellar components of the mergers with gas (contours) have larger maximum values of v/σ and show stronger asymmetries with a clear indication for a change of tilt. Including the gas (assuming it has transformed into stars after the merger was complete), the distribution for equal-mass remnants becomes weakly tilted whereas the distribution for 3:1 remnants shows a clear tilt and extends to a local $v/\sigma \approx 1$ in good agreement with observations.

The lower panels of Figure 16 show the correlation with h_4 . Most collisionless remnants have positive local values of h_4 whereas the remnants with gas show equal amount of positive and negative values. For 3:1 collisionless remnants there is a trend for regions with higher v/σ to have negative h_4 . Adding gas to the analysis results in an over-all shift to more negative values of h_4 .

7 SUMMARY AND DISCUSSION

We have presented a statistical sample of simulations of disc galaxy mergers with a 10% fraction of gas in the progenitor discs. The properties of the merger remnants have been compared to the properties of a similar set of simulations without gas. The effect of star-formation was not included. The presence of a dissipative component changes the shape and the orbital content of the stellar component of the merger remnants. The fraction of box and boxlet orbits which dominate the inner parts of collisionless remnants is significantly reduced if gas is included. The fraction of outer major-axis tubes is reduced as well and inner major-axis tubes disappear completely. In remnants with gas most stars move on minor-axis tube orbits. The change of orbits is caused by gas that settles at the center of the remnants where it deepens the potential well at the same time making it more axisymmetric. In this environment box orbits cannot exist as they are only supported in triaxial potentials. We find that the intermediate axis of the stellar distribution is most strongly affected and the stellar remnants with gas are more axisymmetric. These results are in good qualitative agree-

ment with the findings of Barnes & Hernquist (1996) and Barnes (1998). However, with respect to resolution, statistical completeness and comparison to observations our study goes beyond previous investigations.

The isophotal shape of equal-mass remnants is strongly affected by gas. Around the effective radius minor-axis tubes - as well as box-orbits and boxlets at smaller radii - in the triaxial potential of collisionless remnants support boxy isophotal shapes. In the remnants with gas the fraction of box orbits is reduced and the now dominant tube orbits appear more elliptical or even discy. Statistically, equal-mass mergers with gas do not produce boxy remnants, but they still have a small anisotropy parameter which is in conflict with observations of ellipticals. This is only valid in the limiting case of no starformation during the merger. Realistically, equal-mass disc mergers like nearby ULIRGs do experience bursts of star formation (Genzel et al. 1998, 2001). It is, however, still unclear how much of the available gas is transformed into stars at which stage of the merger. For individual equal-mass merger simulations it has been shown by Bekki & Shioya (1997) and Springel (2000) that boxy remnants can be formed if the star-formation efficiencies were chosen to be high leading to an evolution that is similar to the collisionless case (Naab et al. 1999). Disky remnants form for low efficiencies similar to the results with gas presented here. 3:1 remnants with gas are slightly more discy (see e.g. Bekki 1998 for an unequal-mass merger simulation including star formation) but in general resemble their collisionless counterpart and are in good agreement with observations of discy elliptical galaxies (Bender et al. 1988; Hao et al. 2006) as well as nearby merger remnants (Rothberg & Joseph 2006). We expect that the effect of star formation on the isophotal shape of unequal mass remnants is much weaker (see e.g. Bournaud et al. 2005).

The shape of the LOSVD of the stars is significantly influenced by the presence of gas. Collisionless remnants have LOSVDs which are close to Gaussian or have broad leading wings. In contrast the stellar component of mergers with gas shows a clear tendency for steep leading wings. For remnants with a significant amount of rotation (e.g. 3:1 remnants) this results in an anti-correlation between h_3 and v/σ , especially if the gas component that has formed extended discs is included in the analysis after the merger is complete. This is in good agreement with observations of discy, fast rotating ellipticals (Bender et al. 1994) and might indicate low star-formation efficiencies during the merger event itself. The LOSVDs of equal-mass merger remnants are also consistent with boxy, slowly rotating ellipticals.

If mergers of disc galaxies have indeed formed elliptical galaxies in the not to recent past our results confirm the scenario of Kormendy & Bender (1996) that gas dissipation becomes more important the more discy the isophotes of early-type galaxies are and the faster they rotate. Some equal-mass merger remnants with gas still have a small anisotropy parameter and discy isophotes. Either this conflict with observations can be solved by efficient star formation during the merger or it indicates that massive, boxy ellipticals formed in dissipationless mergers from predominantly stellar progenitors which either were early-type disc galaxies or ellipticals themselves (Naab et al. 1999; Khochfar & Burkert 2003, 2005; González-García & van Albada 2005; Naab et al. 2006). Re-

cent high resolution direct numerical simulations of the formation of field elliptical galaxies from cosmological initial conditions indicate that early-type galaxies after they have formed at high redshift during a phase of intensive merging can thereafter grow by accretion of mainly stellar satellites or minor mergers (Naab et al. 2005).

Combining the results from NB03 and the present study we can conclude that mergers of typical disc galaxies with bulges can have formed giant elliptical of low and intermediate mass in the past. The agreement of kinematic and photometric properties of 1:1 and in particular 3:1 disc mergers with nearby merger remnants is striking. In combination with results from the simulations presented here Dasyra et al. (2006) have been able to show that ongoing disc mergers with ULIRG activity have mass ratios between 1:1 and 3:1. Furthermore the properties of the simulated remnants are in good agreement with the kinematics and isophotal shapes of nearby merger remnants (Rothberg & Joseph 2006). A particularly interesting result is that Rothberg & Joseph (2006) find merger remnants which are discy and anisotropic, a regime that is populated by simulated remnants but not by virialised old elliptical galaxies (see their paper for a detailed discussion). The direct comparison of real nearby mergers with merger simulations are a powerful tool to constrain theories on elliptical galaxy formation and the effect of star formation and black-hole formation (Dasyra et al. 2006) in the local universe which then can be applied to simulations at all redshift ranges.

In the present simulations the conversion of gas into stars has not been included and only progenitors with a small gas fraction have been considered as otherwise neglecting star formation would hardly be justified. We find important signatures of the small gas component in the merger remnants. The question of how stars form and how stellar energetic feedback or central black hole heating affect the multi-phase interstellar medium is still poorly understood (for a summary see e.g. Elmegreen & Scalo 2004), leading to large uncertainties in models of galaxy formation and evolution. Recent simulation e.g. by Springel et al. (2005) and Di Matteo et al. (2005) however demonstrate their importance in understanding the formation of elliptical galaxies in greater details. The orbital content of the remnants will be influenced by the timing of black-hole formation and the efficiency of feedback which determines the amount of gas that can make it to the center leading to the effects presented here. It will be interesting in future work to explore the effect of these processes on the internal orbital structure and projected properties of elliptical galaxies. From a kinematic point of view disc merger remnants appear very similar to observed ellipticals, although questions regarding the age and metallicity of the stellar populations have to be addressed in the future. Analytical models of disc formation (e.g. Naab & Ostriker 2006) which contain all the information about stellar ages and metallicities of the progenitor discs and semi-analytical modeling (Khochfar & Burkert 2005; Khochfar & Silk 2006) in combination with detailed merger simulations (Naab et al. 2006) can be used to place further constraints on the disc merger hypothesis.

ACKNOWLEDGMENTS

This work was supported by the DFG priority program 1177. TN is grateful for interesting discussions with Kalliopi Dasyra, Gregory Novak and Barry Rothberg. He also thanks Barry Rothberg for kindly providing his observational data prior to publication. We thank the referee for valuable comments on the manuscript.

REFERENCES

- Arad I., Johansson P. H., 2005, *MNRAS*, 362, 252
 Barnes J. E., 1992, *ApJ*, 393, 484
 Barnes J. E., 1998, in *Saas-Fee Advanced Course 26: Galaxies: Interactions and Induced Star Formation Dynamics of Galaxy Interactions*. pp 275–+
 Barnes J. E., 2002, *MNRAS*, 333, 481
 Barnes J. E., Hernquist L., 1996, *ApJ*, 471, 115
 Bate M. R., Burkert A., 1997, *MNRAS*, 288, 1060
 Bekki K., 1998, *ApJ*, 502, L133+
 Bekki K., Shioya Y., 1997, *ApJ*, 478, L17+
 Bender R., Doebereiner S., Moellenhoff C., 1988, *A&AS*, 74, 385
 Bender R., Saglia R. P., Gerhard O. E., 1994, *MNRAS*, 269, 785
 Bendo G. J., Barnes J. E., 2000, *MNRAS*, 316, 315
 Binney J., 1978, *MNRAS*, 183, 501
 Binney J., 1985, *MNRAS*, 212, 767
 Binney J., 2005, *MNRAS*, 363, 937
 Bournaud F., Jog C. J., Combes F., 2005, *A&A*, 437, 69
 Burkert A., Naab T., 2005, *MNRAS*, 363, 597
 Carpintero D. D., Aguilar L. A., 1998, *MNRAS*, 298, 1
 Cox T. J., Jonsson P., Primack J. R., Somerville R. S., 2005, *arXiv:astro-ph/0503201*
 Cretton N., Naab T., Rix H.-W., Burkert A., 2001, *ApJ*, 554, 291
 Dasyra K. M., Tacconi L. J., Davies R. I., Genzel R., Lutz D., Naab T., Burkert A., Veilleux S., Sanders D. B., 2006, *ApJ*, 638, 745
 Dasyra K. M., Tacconi L. J., Davies R. I., Naab T., Genzel R., Lutz D., Sturm E., Baker A. J., Veilleux S., Sanders D. B., Burkert A., 2006, *astro-ph/0607468*
 Dehnen W., 2001, *MNRAS*, 324, 273
 Dehnen W., Gerhard O. E., 1994, *MNRAS*, 268, 1019
 Di Matteo T., Springel V., Hernquist L., 2005, *Nature*, 433, 604
 Elmegreen B. G., Scalo J., 2004, *ARA&A*, 42, 211
 R. M., Bacon R., Bureau M., Copin Y., Davies R. L., Krajnović D., Kuntschner H., Miller B. W., de Zeeuw P. T., 2004, *MNRAS*, 352, 721
 Franx M., Illingworth G., de Zeeuw T., 1991, *ApJ*, 383, 112
 Genzel R., Lutz D., Sturm E., Egami E., Kunze D., Moorwood A. F. M., Rigopoulou D., Spoon H. W. W., Sternberg A., Tacconi-Garman L. E., Tacconi L., Thatte N., 1998, *ApJ*, 498, 579
 Genzel R., Tacconi L. J., Rigopoulou D., Lutz D., Tecza M., 2001, *ApJ*, 563, 527
 Gerhard O. E., 1981, *MNRAS*, 197, 179
 Gerhard O. E., 1993, *MNRAS*, 265, 213
 Gerhard O. E., Binney J., 1985, *MNRAS*, 216, 467
 González-García A. C., Balcells M., 2005, *MNRAS*, 357, 753
 González-García A. C., van Albada T. S., 2005, *MNRAS*, 361, 1043
 Hao C. N., Mao S., Deng Z. G., Xia X. Y., Wu H., 2006, *arXiv:astro-ph/0605319*
 Hernquist L., 1990, *ApJ*, 356, 359
 Hernquist L., 1992, *ApJ*, 400, 460
 Hernquist L., 1993, *ApJS*, 86, 389
 Hernquist L., Ostriker J. P., 1992, *ApJ*, 386, 375
 Hernquist L., Spergel D. N., Heyl J. S., 1993, *ApJ*, 416, 415
 Jesseit R., Naab T., Burkert A., 2005, *MNRAS*, 360, 1185
 Jesseit R., Naab T., Peletier R., Burkert A., 2006, *astro-ph/0606144*
 Khochfar S., Burkert A., 2003, *ApJ*, 597, L117
 Khochfar S., Burkert A., 2005, *MNRAS*, 359, 1379
 Khochfar S., Burkert A., 2006, *A&A*, 445, 403
 Khochfar S., Silk J., 2006, *MNRAS*, 370, 902
 Kormendy J., Bender R., 1996, *ApJ*, 464, L119+
 Li Y., Mac Low M.-M., Klessen R. S., 2005, *ApJ*, 620, L19
 Lynden-Bell D., 1967, *MNRAS*, 136, 101
 Merritt D., Fridman T., 1996, *ApJ*, 460, 136
 Mihos J. C., Hernquist L., 1996, *ApJ*, 464, 641
 Naab T., Burkert A., 2001a, in *ASP Conf. Ser. 230: Galaxy Disks and Disk Galaxies Gas Dynamics and Disk Formation in 3:1 Mergers*. pp 451–452
 Naab T., Burkert A., 2001b, *ApJ*, 555, L91
 Naab T., Burkert A., 2003, *ApJ*, 597, 893
 Naab T., Burkert A., Hernquist L., 1999, *ApJ*, 523, L133
 Naab T., Johansson P. H., Efstathiou G., Ostriker J. P., 2005, *astro-ph/0512235*
 Naab T., Khochfar S., Burkert A., 2006, *ApJ*, 636, L81
 Naab T., Ostriker J. P., 2006, *MNRAS*, 366, 899
 Naab T., Trujillo I., 2006, *MNRAS*, 369, 625
 Negroponte J., White S. D. M., 1983, *MNRAS*, 205, 1009
 Pierce M. J., Tully R. B., 1992, *ApJ*, 387, 47
 Rix H., Carollo C. M., Freeman K., 1999, *ApJ*, 513, L25
 Rix H., Franx M., Fisher D., Illingworth G., 1992, *ApJ*, 400, L5
 Rix H.-W., White S. D. M., 1990, *ApJ*, 362, 52
 Robertson B., Cox T. J., Hernquist L., Franx M., Hopkins P. F., Martini P., Springel V., 2006, *ApJ*, 641, 21
 Rothberg B., Joseph R. D., 2006, *arXiv:astro-ph/0604493*
 Schwarzschild M., 1993, *ApJ*, 409, 563
 Scorza C., Bender R., Winkelmann C., Capaccioli M., Macchetto D. F., 1998, *A&AS*, 131, 265
 Springel V., 2000, *MNRAS*, 312, 859
 Springel V., Di Matteo T., Hernquist L., 2005, *ApJ*, 620, L79
 Springel V., Hernquist L., 2005, *ApJ*, 622, L9
 Toomre A., Toomre J., 1972, *ApJ*, 178, 623
 Tremaine S., Gebhardt K., Bender R., Bower G., Dressler A., Faber S. M., Filippenko A. V., Green R., Grillmair C., Ho L. C., Kormendy J., Lauer T. R., Magorrian J., Pinkney J., Richstone D., 2002, *ApJ*, 574, 740
 Valluri M., Merritt D., 1998, *ApJ*, 506, 686
 van der Marel R. P., Franx M., 1993, *ApJ*, 407, 525
 Wagner S. J., Bender R., Moellenhoff C., 1988, *A&A*, 195, L5
 Weil M. L., Hernquist L., 1996, *ApJ*, 460, 101

Wetzstein M., Naab T., Burkert A., 2005, arXiv:astro-ph/0510821